Earth and Planetary Science Letters 499 (2018) 243–255

Contents lists available at ScienceDirect

Earth and Planetary Science Letters

www.elsevier.com/locate/epsl

Structural control on earthquake behaviors revealed by high-resolution V_p/V_s imaging along the Gofar transform fault, East Pacific Rise

Hao Guo [a], Haijiang Zhang [a,*], Berenice Froment [b]

[a] Laboratory of Seismology and Physics of Earth's Interior, School of Earth and Space Sciences, University of Science and Technology of China, Hefei, Anhui, China
[b] Institut de Radioprotection et de Sûreté Nucléaire (IRSN), Fontenay-aux-Roses, France

ARTICLE INFO

Article history:
Received 12 February 2018
Received in revised form 23 July 2018
Accepted 24 July 2018
Available online xxxx
Editor: M. Ishii

Keywords:
oceanic transform fault
temporal and spatial earthquake evolution
fault segmentation
double-difference tomography
V_p/V_s inversion

ABSTRACT

The Gofar transform fault (GTF), 4°S on the East Pacific Rise, can generate M_w 5.5–6 earthquakes quasiperiodically on some specific patches that are separated by stationary rupture barriers. Small earthquakes along strike show a clear spatial and temporal evolution. To better understand the cause of the observed behaviors of large and small earthquakes, we have determined high-resolution earthquake locations within a period of one year covering the 2008 M_w 6.0 (M6) earthquake, as well as V_p, V_s, and V_p/V_s models along the westernmost segment of the GTF, using a well recorded ocean bottom seismograph dataset and a new V_p/V_s model consistency-constrained double-difference tomography method. Compared to the previous P-wave tomography study in this area, the use of a new automatic arrival picking algorithm significantly improves the accuracy of S-wave arrival times, thereby allowing for the inversion of V_s and V_p/V_s models in addition to V_p model. High-precision waveform cross-correlation differential times are also used. The tomographic V_p/V_s model reveals strong structural variations at multiple scales along the fault, which likely control the behaviors of large and small earthquakes. The M6 mainshock is generated within a specific ∼8-km-long fault patch composed of intact rocks. By contrast, multiple fluid-filled damaged zones on both sides of this asperity are imaged and have varying size which is suggested to be critical in their ability of stopping ∼M6 ruptures. High-resolution earthquake relocations and velocity models also indicate that the occurrence of small earthquakes is also correlated with structural variations. Combined with previous studies, our results further suggest that strong structural variations control the fault mechanics and earthquake behavior along the GTF.

1. Introduction

Faults can slip in different modes, including slow slip, non-volcanic tremor, steady creep, microseismicity, and large dangerous earthquakes (Ide et al., 2007; Peng and Gomberg, 2010), but our understanding of their physical mechanisms is still very limited (Harris, 2017). In contrast to continental faults, mid-ocean ridge transform faults (RTFs) provide a better tectonic environment for studying how fault zone physical properties influence fault slip and earthquake behaviors because they have relatively simple geometries with average slip rates that are well defined by plate spreading velocities, and show, in general, more homogeneous compositions and more predictable thermal structures (Boettcher and Jordan, 2004; Roland et al., 2012).

The Gofar transform fault (GTF), located 4°S on the East Pacific Rise (EPR), has three fault segments (G1, G2, and G3) separated by intratransform spreading centers (Fig. 1a) and can generate M_w ∼6 (M6) earthquakes quasiperiodically every 5 to 6 years on some specific fault patches (McGuire, 2008). In this study, we focus on the short (∼90 km) and high-slip-rate (∼14 cm/yr) westernmost segment (G3) of the GTF (Fig. 1a). The G3 has two distinct asperity patches (red and orange ellipses in Fig. 1b) that repeatedly generate M6 earthquakes and are separated by a stationary rupture barrier patch that can stop the propagation of M6 earthquakes (Fig. 1b) (McGuire et al., 2012).

In 2008, motivated by the observed regular EPR seismic cycles (McGuire, 2008), Woods Hole Oceanographic Institution (WHOI) deployed 16 ocean bottom seismographs (OBS) around the G3 fault segment for one year of continuous monitoring. This experiment successfully captured a M6 earthquake that occurred on 18 September 2008 on G3 (red star in Fig. 1b) (McGuire et al., 2012). In addition, a wide-angle seismic refraction survey line was also

* Corresponding author.
E-mail addresses: hguo@mail.ustc.edu.cn (H. Guo), zhang11@ustc.edu.cn (H. Zhang), berenice.froment@irsn.fr (B. Froment).

https://doi.org/10.1016/j.epsl.2018.07.037

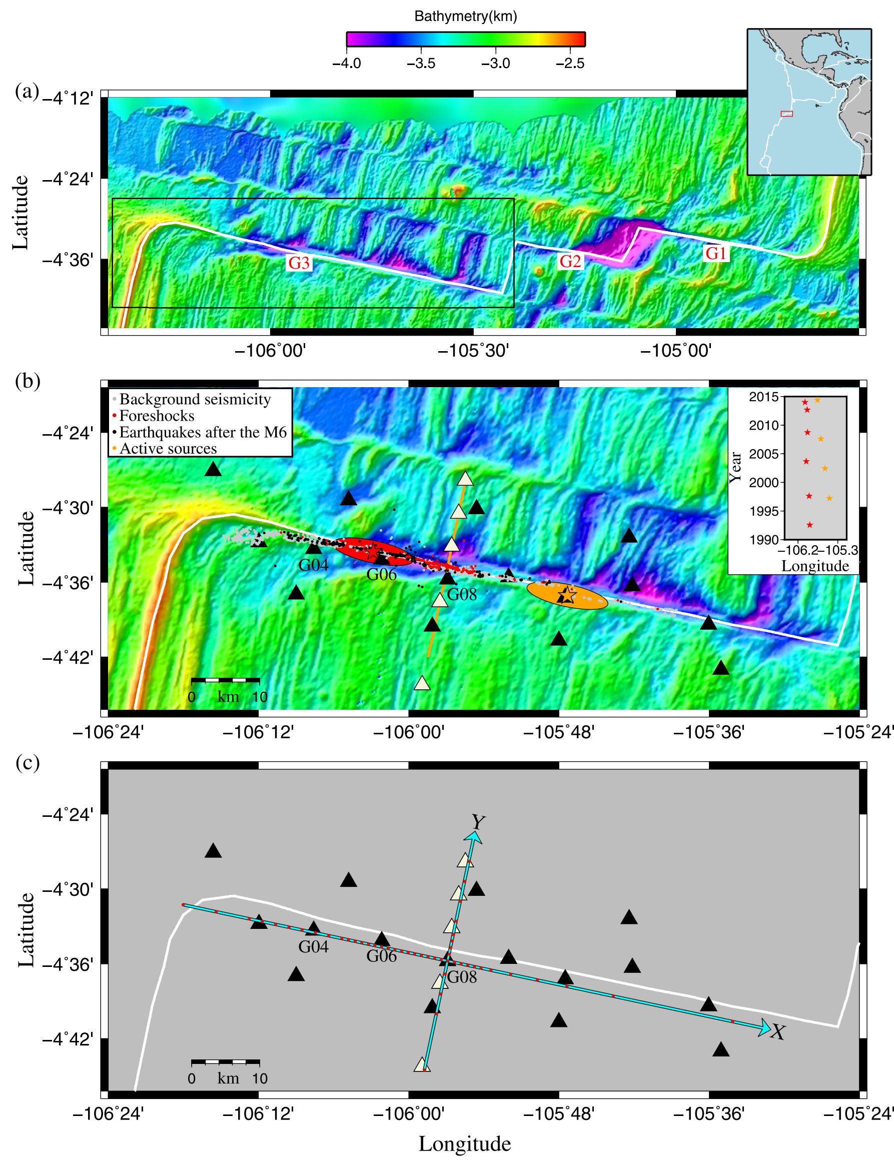

Fig. 1. (**a**) Gofar transform fault system, including three fault segments (G1, G2, and G3) separated by intratransform spreading centers. The black rectangle outlines the G3 segment shown in Fig. 1b. White line shows the plate boundary. The inset map in the upper-right corner shows the geographic location of the GTF. (**b**) Distribution of earthquakes and stations around G3. Black triangles represent the OBS sites deployed for the one-year passive-source experiment in 2008, among which stations G04, G06 and G08 are labeled. Beige triangles represent the OBS sites deployed for the active-source experiment. Orange dots forming a line represent the active-source air-gun shots across the fault. Grey, red, and black dots represent the relocations of background earthquakes, foreshocks, and the earthquakes after the mainshock with small location uncertainties, respectively. Note that compared to Fig. 6a, here the relocations after the mainshock are within 20 days after the mainshock. Red and orange ellipses represent ∼10-km-long asperity patches centered on the centroid locations of the 2008 M_w 6.0 (red star) and 2007 M_w 6.2 (orange star) mainshocks, respectively. The centroid locations of these two M6 mainshocks were determined by McGuire et al. (2012). As shown in the temporal evolution plot in the upper-right, these two patches generate large earthquakes (i.e. red and orange stars in the upper-right plot) every ∼5–6 years (note that the locations of these large earthquakes are from GCMT catalog, which has relatively large location uncertainties. See McGuire (2008) for details on how the overlapping rupture patches of these large earthquakes are defined). (**c**) Horizontal Cartesian coordinate system and grid setting for the inversion. The X and Y axes of the Cartesian coordinate system are represented by cyan lines, with arrows pointing to the positive directions. The coordinate center is located at G08. The Y axis is rotated 12° clockwise from North so that the X axis is parallel to the fault strike. The grid nodes (red dots) on the coordinate axis are positioned at $X = -40, -35, -30, -28, -26, -24, -22, -20, -18, -16, -15, -14, -13, -12, -11, -10, -9, -8, -7, -6, -5, -4, -3, -2$ $-1, 0, 1, 2, 3, 4, 5, 6.5, 9.5, 13.5, 18, 25, 43$ km, and $Y = -16.5\ -8, -5, -2, 0, 1, 2, 3, 4, 6, 9, 12, 15$ km. Note that the G3 active fault trace is at about $Y = 2$ km. (For interpretation of the colors in the figure(s), the reader is referred to the web version of this article.)

conducted across the rupture barrier patch (Fig. 1b) (Roland et al., 2012).

Using the 2008 1-year-long OBS array dataset, McGuire et al. (2012) detected and located tens of thousands of earthquakes, including a 1-week-long sequence of foreshocks preceding the 2008 M6 mainshock, aftershocks, an earthquake swarm that occurred in December, as well as the background seismicity that occurred before foreshocks (Fig. 1b). This 1-year-long seismicity showed along-strike variations in earthquake rupture properties. McGuire et al. (2012) suggested that the ∼10-km rupture barrier patch (defined as Patch 1 in this paper), associated with abundant foreshocks and deep seismicity, could stop the mainshock rupture, probably as a result of enhanced fluid circulation.

Using the active-source seismic dataset, Roland et al. (2012) determined a 2-D P-wave tomography model across the fault, which just passed through the rupture barrier patch (Fig. 1). A low-velocity fault zone throughout the crust was imaged and interpreted to be highly damaged with enhanced fluid-filled porosity (Roland et al., 2012).

Combining both datasets, Froment et al. (2014) complemented the work of Roland et al. (2012) by determining the along-strike V_p model using the double-difference (DD) tomography method